Luminescence Properties of Eu^{2+}-Activated Alkaline-Earth Silicon-Oxynitride $MSi_2O_{2-\delta}N_{2+2/3\delta}$ (M = Ca, Sr, Ba): A Promising Class of Novel LED Conversion Phosphors

Y. Q. Li, A. C. A. Delsing, G. de With, and H. T. Hintzen*

Laboratory of Materials and Interface Chemistry, Department of Chemical Engineering and Chemistry, Eindhoven University of Technology, P.O. Box 513, 5600 MB Eindhoven, The Netherlands

Received January 25, 2005. Revised Manuscript Received March 30, 2005

The luminescence properties of Eu^{2+}-activated alkaline-earth silicon-oxynitrides have been studied. In the $BaO-SiO_2-Si_3N_4$ system, a new $BaSi_2O_2N_2$ compound was obtained having the monoclinic structure with lattice parameters $a = 14.070(4)$ Å, $b = 7.276(2)$ Å, $c = 13.181(3)$ Å, $\beta = 107.74(6)°$. All $MSi_2O_{2-\delta}N_{2+2/3\delta}:Eu^{2+}$ (M = Ca, Sr, Ba) materials can be efficiently excited in the UV to visible region (370−460 nm), making them attractive as conversion phosphors for LED applications. A blue-green emission at 490−500 is observed for $BaSi_2O_2N_2:Eu^{2+}$, yellow emission at 560 nm for $CaSi_2O_{2-\delta}N_{2+2/3\delta}:Eu^{2+}$ ($\delta \approx 0$), and a green-yellow emission peaking from 530 to 570 nm for $SrSi_2O_{2-\delta}N_{2+2/3\delta}:Eu^{2+}$ ($\delta \approx 1$), the position depending on the exact value of δ. $BaSi_2O_2N_2:Eu^{2+}$ is the most promising conversion phosphor for white-light LEDs due to its high conversion efficiency for blue light from InGaN-based LEDs related to its very small Stokes shift.

1. Introduction

Since the invention of blue emitting InGaN-based white-light-diodes (LED), the efficiency of white-light LEDs has been improved significantly. So far, the efficiency of white-light LEDs has already surpassed that of incandescent lamps and is competitive with fluorescent lamps. White-light LEDs show high potential for replacement of conventional lighting like incandescent and fluorescent lamps, the advantages being its long lifetime, saving energy consumption, and its environmental-friendly characteristics.[1−5] White-light LEDs can be realized by combining a InGaN-based diode with phosphor materials, like $YAG:Ce^{3+}$, from which white light is then produced by additive mixing of yellow light emitted by the phosphor with blue light from the LED. Therefore, the phosphor materials play an important role in white-light LEDs. However, with respect to the presently used phosphors in white-light LED systems, most of them do not meet the optimum requirements of white-light LEDs. For example, $YAG:Ce^{3+}$ shows a high thermal quenching and a poor color rendition, which can be improved by sulfide-based phosphors (i.e., red, $SrS:Eu^{2+}$ and $CaS:Eu^{2+}$; green, $SrGa_2S_4:Eu^{2+}$). However, these sulfide materials suffer from low chemical stability in LEDs environment. Ideally the conversion phosphors for white-light LEDs must combine a high quantum efficiency and absorption for UV-blue radiation with the ability to withstand the high temperature generated by the LED without degrading and quenching the luminescence, and moreover should be chemically stable. Thus, novel phosphor materials with improved properties are greatly in demand.

Recently, some nitride-based phosphor materials have been invented with unconventional properties for use in white-light LEDs.[6−16] Among these phosphors, Eu^{2+}-activated $M_2Si_5N_8$ (M = Ca, Sr, Ba) is a new family of divalent europium doped red- or red-orange-emitting alkaline-earth silicon nitride materials, which has proved to be excellent phosphor materials for white-light LED application.[10,17,18] However, very few efficient new phosphors with yellow and green emission have actually been found for white-light LEDs. As expected, the performances of white-light LEDs, such as the color rendition index (CRI), color temperature, and color

* Corresponding author. Tel.: +31 40 2472770. Fax: +31 40 2445619. E-mail: h.t.hintzen@tue.nl.

(1) Nakamura, S. *Appl. Phys. Lett.* **1994**, *64*, 1687.
(2) Aanegola, S.; Petroski, J.; Radkov, E. *SPIE* **2003**, *10*, 16.
(3) Narukawa, Y. *Optics & Photonics News* **2004**, *4*, 25.
(4) Rohwer, L. S.; Srivastava, A. M. *Electrochem. Soc. Interface* **2003**, *12*, 36.
(5) Taso, J. Y.; Ed. *Light Emitting Diodes (LEDs) for General Illumination Update 2002*; Optoelectronics Industry Development Association: Washington, DC, 2002.
(6) Hintzen, H. T.; Li, Y. Q. *Encyclopedia of Materials: Science and Technology* **2004**, 1.
(7) van Krevel, J. W. H. Ph.D. Thesis, Eindhoven University of Technology, 2000.
(8) van Krevel, J. W. H.; Hintzen, H. T.; Metselaar, R.; Meijerink, A. *J. Alloys Compd.* **1998**, *268*, 272.
(9) van Krevel, J. W. H.; Hintzen, H. T.; Metselaar, R. *Mater. Res. Bull.* **2000**, *35*, 747.
(10) Hintzen, H. T.; van Krevel, J. W. H.; Botty, G. European Patent EP 1104799 A1, 1999.
(11) Hoppe, H. A.; Morys, H.; Lutz, P.; Schnick, W.; Seilmeier, A. *J. Phys. Chem. Solids* **2000**, *61*, 2001.
(12) van Krevel, J. W. H.; van Rutten, J. W. T.; Mandal, H.; Hintzen, H. T.; Metselaar, R. *J. Solid State Chem.* **2002**, *165*, 19.
(13) Li, Y. Q.; De With, G.; Hintzen, H. T. *J. Alloys Compd.* **2004**, *385*, 1.
(14) Li, Y. Q.; De With, G.; Hintzen, H. T. *J. Solid State Chem.* **2004**, *177*, 4687.
(15) Yamada, M.; Naitou, T.; Izuno, K.; Tamaki, H.; Murazaki, Y.; Kameshima, M.; Mukai, T. *Jpn. J. Appl. Phys.* **2003**, *42*, L20.
(16) Xie, R. J.; Hirosaki, N.; Sakuma, K.; Yamamoto, Y.; Mitomo, M. *Appl. Phys. Lett.* **2004**, *84*, 5404.
(17) Tamaki, H.; Kameshima, M.; Takashima, S.; Yamada, M.; Naitou, T.; Sakai, K.; Murazaki, Y. European Patent EP 1433831 A1, 2003.
(18) Juestel, T.; Schmidt, T.; Hoeppe, H.; Schnick, W.; Mayr, W. PCT WO 2004/055910 A1.

10.1021/cm050175d CCC: $30.25
Published on Web 05/20/2005

range, can be significantly improved by combination of the above-mentioned red emitting phosphors and a green emitting phosphor together with the blue light source from a InGaN-chip.

In contrast to the recently found alkaline-earth silicon-nitride compounds $M_2Si_5N_8$ (M = Ca, Sr, Ba), several alkaline-earth silicon-oxynitride compounds, that is, $CaSi_2O_2N_2$ and $SrSi_2O_2N_2$, were reported earlier in the CaO−Si_3N_4−AlN and Sr−Si−O−N systems, respectively.[19−21] Just recently, a single-crystal structure determination was published for $CaSi_2O_2N_2$.[22] However, the luminescence properties of rare-earth doped $CaSi_2O_2N_2$ and $SrSi_2O_2N_2$ have not been reported yet. Additionally, further extending to the Ba−Si−O−N system is also very interesting like in the case of the alkaline-earth silicates[23−28] and alkaline-earth silicon nitrides.[6,10,11] In the present study, we therefore focus on the preparation and luminescence properties of Eu^{2+}-doped $MSi_2O_{2-\delta}N_{2+2/3\delta}$ (M = Ca, Sr, Ba) compounds aiming at exploring new oxynitride-based phosphors for use in white-light LEDs.

2. Experimental Section

2.1. Preparation. All powder samples of undoped and Eu^{2+}-doped $MSi_2O_{2-\delta}N_{2+2/3\delta}$ (M = Ca, Sr, Ba) were synthesized by a high-temperature solid-state reaction. The starting materials were high-purity MCO_3 (M = Ca, Sr, Ba) (Merck, > 99.0%), SiO_2 (Aerosil OX 50, Degussa), Si_3N_4 (SKW Trostberg, β content: 23.3%, O ~0.7%), and Eu_2O_3 (Rhône-Poulenc, 99.99%). The Eu^{2+} mole fractions with respect to the M^{2+} ion range from 1% (x = 0.01) to 10% (x = 0.1). The starting materials were weighed out in various amounts (keeping the M/Si ratio constant to 0.5), and subsequently homogeneously wet-mixed by a planetary ball mill for 4−5 h in 2-propanol. After mixing, the slurry was dried and ground in an agate mortar. Subsequently, the dried powder mixtures were fired in molybdenum or alumina crucibles at 1100−1400 °C for 6−12 h under a reducing atmosphere of N_2−H_2 (10%) in horizontal tube furnaces. After firing, the samples were cooled to room temperature in the furnace and were ground again with an agate mortar.

2.2. X-ray Powder Diffraction. All final products were checked by X-ray powder diffraction (Rigaku, D/MAX-B) using Cu Kα radiation at 40 kV and 30 mA with a graphite monochromator. For phase identification, a normal scan (2°/min) was performed. The crystallographic data were collected on the powder samples using a step scan mode with a step size of 0.02° and a counting time of 10 s per step in the range 2θ 10°−90°. To avoid the preferred orientation of the obtained samples, the powder samples were mounted into a flat plate holder by the side filling method.

Table 1. Lattice Parameters of $MSi_2O_{2-\delta}N_{2+2/3\delta}$ (M = Ca, Sr, Ba)

formula	$CaSi_2O_2N_2$ ($\delta \approx 0$)	$SrSi_2ON_{8/3}$ ($\delta \approx 1$)	$BaSi_2O_2N_2$ ($\delta = 0$)
crystal system	monoclinic	monoclinic	monoclinic
space group	$P2_1/c$	$P2_1/m$	P_2/m
lattice constants			
a (Å)	15.035(4)	11.320(4)	14.070(4)
b (Å)	15.450(1)	14.107(6)	7.276(2)
c (Å)	6.851(2)	7.736(4)	13.181(3)
β (deg)	95.26(3)	91.87(3)	107.74(6)
V (Å^3)	1584.53	1234.67	1285.23
figure-of-merit			
M(20)	10.5	10.8	10.3
F(20)	15.7(0.0088, 144)	14.9(0.0090, 150)	15.4(0.0095, 137)

The unit cell of $MSi_2O_{2-\delta}N_{2+2/3\delta}$ was determined from the X-ray powder diffraction patterns using indexing programs DICVOL04[29] for M = Ca, Sr and McMaill[30] (an indexing program for X-ray powder diffraction based on Monte Carlo and grid search) for M = Ba based on the first 20 lines for the search of solutions. The possible space groups are determined according to the systematic absences, and the obtained unit cells are further examined by fitting the full profile X-ray powder diffraction patterns using the Le Bail method[31] within the program GSAS.[32,33]

2.3. Optical Measurements. The diffuse reflectance, emission, and excitation spectra of the samples were obtained at room temperature by a Perkin-Elmer LS 50B spectrophotometer equipped with a Xe flash lamp. The reflection spectra were calibrated with the reflection of black felt (reflection 3%) and white barium sulfate ($BaSO_4$, reflection ~100%) in the wavelength region of 230−700 nm. The excitation and emission slits were set at 2.5 nm. The emission spectra were corrected by dividing the measured emission intensity by the ratio of the observed spectrum of a calibrated W-lamp and its known spectrum from 300 to 900 nm. Excitation spectra were automatically corrected for the variation in the lamp intensity by a second photomultiplier and a beam-splitter. All of the spectra were measured with a scan speed of 100 nm/min. Further, the quantum efficiency (400 nm, 460 nm) was determined as compared to the standard materials.

3. Results and Discussion

3.1. Phase Identification. In the BaO−SiO_2−Si_3N_4 system, we obtained a single-phase compound with an approximate composition $BaSi_2O_2N_2$, which crystallizes in the monoclinic crystal system with the lattice parameters: a = 14.070(4) Å, b = 7.276(2) Å, c = 13.181(3) Å, β = 107.74-(6)° (Table 1). The X-ray powder diffraction data are given in Table 2. For the CaO−SiO_2−Si_3N_4 system, $CaSi_2O_2N_2$ was formed as a nearly single-phase material with always some traces of Ca_2SiO_4 and $CaSiO_3$. This suggests that the composition of $CaSi_2O_{2-\delta}N_{2+2/3\delta}$ probably may be somewhat more nitrogen rich than $CaSi_2O_2N_2$, that is, $\delta \geq 0$. This is supported by the fact that the $CaSi_2O_2N_2$ compound reported in the literature was prepared from CaO−Si_3N_4 mixtures.[22] A similar, but more profound, behavior was found for the SrO−SiO_2−Si_3N_4 system, where we could only obtain almost

(19) Huang, Z. K.; Sun, W. Y.; Yan, D. S. *J. Mater. Sci. Lett.* **1985**, *4*, 255.
(20) Zhu, W. H.; Wang, P. L.; Sun, W. Y.; Yan, D. S. *J. Mater. Sci. Lett.* **1994**, *13*, 560.
(21) Cao, G. Z.; Huang, Z. K.; Fu, X. R.; Yan, D. S. *Int. J. High Technol. Ceram.* **1986**, *2*, 115.
(22) Höppe, H. A.; Stadler, F.; Oeckler, O.; Schnick, W. *Angew. Chem., Int. Ed.* **2004**, *43*, 5540.
(23) Poort, S. H. M.; Janssen, W.; Blasse, G. *J. Alloys Compd.* **1997**, *260*, 93.
(24) Poort, S. H. M.; Reijnhoudt, H. M.; van der Kulp, H. O. T.; Blasse, G. *J. Alloys Compd.* **1996**, *241*, 75.
(25) Poort, S. H. M.; Meyerink, A.; Blasse, G. *J. Phys. Chem. Solids* **1997**, *58*, 1451.
(26) Kim, J. S.; Kang, J. Y.; Jeon, P. E.; Choi, J. C.; Park, H. L.; Kim, T. W. *Jpn. J. Appl. Phys.* **2004**, *43*, 989.
(27) Kim, J. S.; Jeon, P. E.; Choi, J. C.; Park, H. L. *Solid State Commun.* **2005**, *133*, 187.
(28) Kim, J. S.; Park, Y. H.; Kim, S. M.; Choi, J. C.; Park, H. L. *Solid State Commun.* **2005**, *133*, 445.
(29) Boultif, A.; Louer, D. *J. Appl. Crystallogr.* **2004**, *37*, 724.
(30) Le Bail, A. http://www.cristal.org/McMaille/.
(31) Le Bail, A; Duroy, H.; Fourquet, J. L. *Mater. Res. Bull.* **1988**, *23*, 447.
(32) Larson, A. C.; Von Dreele, R. B. Report LAUR 86-748, Los Alamos National Laboratory, Los Alamos, NM, 2000.
(33) Toby, B. H. *J. Appl. Crystallogr.* **2001**, *34*, 210.

Table 2. X-ray Powder Diffraction Data for $BaSi_2O_2N_2$

h	*k*	*l*	d_{obs} (Å)	$2\theta_{obs}$ (deg)	$2\theta_{cal}$ (deg)	$\Delta 2\theta$ (deg)	I/I_o (%)
0	1	0	7.2725	12.1600	12.1546	−0.0062	84.7
−2	0	1	6.8465	12.9200	12.9325	−0.0240	20.2
0	1	1	6.3261	13.9880	14.0572	−0.0808	<1
2	0	1	5.2790	16.7800	16.7757	−0.0072	<1
−3	0	1	4.6402	19.1110	18.9342	0.1653	2.3
−3	0	2	4.3143	20.5700	20.5774	−0.0189	2.6
−2	1	3	3.6144	24.6100	24.6085	−0.0098	100.0
0	2	1	3.4942	25.4700	25.4713	−0.0126	36.0
−1	2	1	3.4543	25.7700	25.7773	−0.0187	4.5
3	1	1	3.4050	26.1500	26.1446	−0.0059	20.8
4	0	0	3.3558	26.5400	26.5853	−0.0567	5.9
−2	2	1	3.2098	27.7700	27.7529	0.0058	21.0
−1	1	4	2.9937	29.8200	29.8079	0.0008	29.8
0	1	4	2.8815	31.0100	31.0061	−0.0074	80.8
5	0	0	2.6797	33.4100	33.4056	−0.0067	22.2
0	0	5	2.5116	35.7200	35.7313	−0.0224	12.7
4	1	2	2.4827	36.1500	36.1625	−0.0235	6.2
−2	2	4	2.4225	37.0800	37.0784	−0.0094	21.5
3	2	2	2.4044	37.3690	37.3496	0.0083	14.3
−5	1	4	2.3104	38.9500	38.9341	0.0049	4.0
4	0	3	2.2963	39.2000	39.2018	−0.0128	6.9
1	2	4	2.2495	40.0500	39.9989	0.0402	28.0
−3	3	1	2.1494	42.0000	41.9154	0.0737	7.0
−3	3	0	2.1310	42.3800	42.3736	−0.0044	9.7
0	3	3	2.0966	43.1100	43.0737	0.0254	5.7
2	3	2	2.0715	43.6600	43.5730	0.0762	1.6
−7	0	2	2.0095	45.0800	45.0693	−0.0000	10.6
3	0	5	1.9478	46.5910	46.5426	0.0377	4.3
2	3	3	1.9206	47.2890	47.2928	−0.0145	1.4
−5	3	1	1.8371	49.5800	49.6847	−0.1152	6.5
−3	1	7	1.8148	50.2300	50.2511	−0.0316	1.4
−1	4	0	1.8017	50.6200	50.6018	0.0077	5.0
−1	4	1	1.7945	50.8400	50.8410	−0.0115	13.1
5	0	4	1.7863	51.0900	51.0711	0.0083	26.6
−2	4	0	1.7534	52.1200	52.0567	0.0528	3.6
0	1	7	1.7416	52.5000	52.5091	−0.0195	7.7
3	0	6	1.7046	53.7300	53.6943	0.0253	4.9
−3	4	1	1.6973	53.9800	54.0411	−0.0715	2.2
−7	0	6	1.6889	54.2700	54.1507	0.1089	<1
−6	3	3	1.6620	55.2200	55.2538	−0.0441	4.6
5	3	2	1.6386	56.0800	55.9491	0.1207	13.7
−4	4	2	1.6061	57.3200	57.3267	−0.0169	4.9
−4	4	0	1.5997	57.5690	57.6168	−0.0580	1.6
−4	3	6	1.5799	58.3600	58.3587	−0.0089	5.4
1	2	7	1.5504	59.5800	59.6896	−0.1197	2.3
1	4	4	1.5352	60.2300	60.1958	0.0242	3.9
3	0	7	1.5107	61.3100	61.2289	0.0711	<1
−1	4	5	1.4932	62.1100	62.0983	0.0017	3.3
5	2	5	1.4696	63.2200	63.2934	−0.0833	7.7
6	0	5	1.4618	63.6000	63.5824	0.0078	5.3
−1	5	0	1.4461	64.3700	64.3456	0.0145	4.3
−7	2	7	1.4403	64.6600	64.6476	0.0025	10.2
4	4	3	1.4258	65.4010	65.4031	−0.0119	1.1
−6	4	0	1.4098	66.2400	66.2085	0.0218	<1
−10	0	2	1.3999	66.7690	66.7334	0.0258	<1
−1	5	3	1.3803	67.8400	67.7859	0.0445	3.3
−10	1	4	1.3711	68.3610	68.3952	−0.0439	1.9
−2	3	8	1.3603	68.9800	68.9807	−0.0103	3.5
2	3	7	1.3435	69.9690	69.9599	−0.0005	<1
9	1	2	1.3361	70.4100	70.4387	−0.0382	<1
−10	0	6	1.3263	71.0100	70.9743	0.0263	2.8
−4	0	10	1.3138	71.7900	71.7456	0.0350	2.0
1	5	4	1.2976	72.8300	72.8261	−0.0055	2.3
−6	4	6	1.2901	73.3190	73.3167	−0.0071	<1
3	3	7	1.2828	73.8090	73.7669	0.0328	<1
3	2	8	1.2708	74.6210	74.5857	0.0261	4.8
−6	1	10	1.2528	75.8810	75.8409	0.0309	<1
−8	4	4	1.2454	76.4100	76.3822	0.0186	<1
−7	0	10	1.2368	77.0400	77.0496	−0.0187	5.3
−6	4	7	1.2298	77.5600	77.5854	−0.0345	1.8
2	2	9	1.2151	78.6800	78.6604	0.0106	2.6
−1	5	6	1.2086	79.1890	79.1837	−0.0037	1.1
−11	2	2	1.1995	79.9090	79.9124	−0.0123	<1
−10	3	5	1.1911	80.5900	80.5568	0.0243	2.7
4	5	4	1.1777	81.7000	81.6880	0.0032	2.1
−5	5	6	1.1692	82.4200	82.4023	0.0090	<1

Table 2 (Continued)

h	k	l	d_{obs} (Å)	$2\theta_{obs}$ (deg)	$2\theta_{cal}$ (deg)	$\Delta 2\theta$ (deg)	I/I_o (%)
−12	0	5	1.1596	83.2510	83.2207	0.0216	1.4
1	2	10	1.1541	83.7400	83.8131	−0.0818	2.6
−12	1	5	1.1455	84.5100	84.5126	−0.0112	<1
2	3	9	1.1384	85.1600	85.1509	0.0005	<1
−4	6	3	1.1302	85.9300	85.9273	−0.0058	<1
3	0	10	1.1222	86.6900	86.6400	0.0416	2.3
−12	0	7	1.1123	87.6600	87.6793	−0.0277	1.6
−6	4	9	1.1035	88.5400	88.5323	−0.0007	1.3
10	3	2	1.1011	88.7800	88.7791	−0.0074	1.1
−10	4	1	1.0980	89.1010	89.0879	0.0048	<1
−9	2	10	1.0943	89.4790	89.4885	−0.0177	<1

Table 3. Excitation and Emission Bands, Crystal Field Splitting, and Center of Gravity of the 5d Level as Well as the Stokes Shift of $M_{0.9}Eu_{0.1}Si_2O_{2-\delta}N_{2+2/3\delta}$ and the Absorption Edge of Undoped $MSi_2O_{2-\delta}N_{2+2/3\delta}$ (M = Ca, Sr, Ba)

M	excitation band (nm)	emission band (nm)	absorption edge[a] (nm)	crystal field splitting (cm^{-1})	center of gravity (cm^{-1})	Stokes shift (cm^{-1})
Ca	259, 341, 395, 436	560	∼280	∼15 700	∼29 000	∼5100
Sr	260, 341, 387, 440	530−570	∼270	∼15 700	∼29 100	∼3900−5200
Ba	264, 327, 406, 460	499	∼240	∼16 100	∼28 700	∼1700

[a] Undoped $MSi_2O_{2-\delta}N_{2+2/3\delta}$.

single-phase material when completely omitting the SiO_2 starting material and just starting with only SrO and Si_3N_4. The approximate composition of this strontium silicon oxynitride compound thus is $SrSi_2ON_{8/3}$ ($\delta \approx 1$).

Figure 1 shows the observed and simulated powder diffraction pattern of the most pure $MSi_2O_{2-\delta}N_{2+2/3\delta}$ (M = Ca, Sr, Ba) compounds. All $MSi_2O_{2-\delta}N_{2+2/3\delta}$ compounds crystallize in a monoclinic unit cell but with different space groups and lattice parameters for M = Ca, Sr, Ba (Table 1).[34] It is evident that the structure of $BaSi_2O_2N_2$ is different from that of $MSi_2O_{2-\delta}N_{2+2/3\delta}$ (M = Ca, Sr), showing resemblances for Ca and Sr. Although the powder diffraction patterns of $MSi_2O_{2-\delta}N_{2+2/3\delta}$ (M = Ca, Sr) are essentially close to those previously reported for $CaSi_2O_2N_2$ and $SrSi_2O_2N_2$ (low-temperature form),[20,21] we found that these data are inexact related to missing peaks and wrong indexing. In addition, the XRD pattern belonging to the $MSi_2O_{2-\delta}N_{2+2/3\delta}$ (M = Ca, Sr) compound depends on the composition of the starting mixture. For example, for the nitrogen-rich $SrSi_2O_{2-\delta}N_{2+2/3\delta}$ ($\delta \approx 1$) samples, the strongest peak is at about 25.35° 2θ with the smallest amount of second phases. In reverse, for oxygen-rich $SrSi_2O_{2-\delta}N_{2+2/3\delta}$ ($\delta \approx 0$) the strongest peak is located at 31.69° 2θ. The XRD data of our $CaSi_2O_{2-\delta}N_{2+2/3\delta}$ ($\delta \approx 0$) powder sample could not be successfully refined with the structural parameters determined for a $CaSi_2O_2N_2$ single crystal by Höppe et al.[22] Probably several modifications of $CaSi_2O_2N_2$ exist depending on the temperature (the powder was prepared at 1400 °C, while the single crystal was obtained by raising the temperature up till 1900 °C[22]), similar to what is also found for $SrSi_2O_{2-\delta}N_{2+2/3\delta}$.[20]

3.2. Luminescence of Eu^{2+}-Doped $MSi_2O_{2-\delta}N_{2+2/3\delta}$ (M = Ca, Sr, Ba). The daylight color of the undoped alkaline-earth silicon oxynitrides is gray-white. Therefore, $MSi_2O_{2-\delta}N_{2+2/3\delta}$ (M = Ca, Sr, Ba) shows a high reflection in the visible range (400−650 nm) and a sharp drop between 250 and 300 nm (Figure 2), which corresponds to the host lattice excitation. Accordingly, the estimated absorption edge of the undoped materials is around 240−280 nm (4.4−5.2 eV) (Table 3). Figure 2 also shows the diffuse reflection spectra of the Eu-doped compounds. Clearly, these refection spectra illustrate that the absorption bands of Eu^{2+} extend into the visible region. The onset of the absorption bands for the compounds doped with 10% Eu is around 490 nm for M = Ca, 585 nm for M = Sr, and 500 nm for M = Ba.

Excitation and emission spectra for 10 mol % Eu^{2+}-doped $MSi_2O_{2-\delta}N_{2+2/3\delta}$ (M = Ca, Sr, Ba) are depicted in Figure 3. The excitation spectra of $M_{0.9}Eu_{0.1}Si_2O_{2-\delta}N_{2+2/3\delta}$ (M = Ca, Sr, Ba) are consistent with the corresponding reflection spectra (Figure 2) and show a number of broad bands corresponding to the crystal-field components of the 5d level in the excited $4f^65d$ configuration of the Eu^{2+} ion (see Table 3). From Table 3, it can be clearly seen that the position of the excitation bands is very similar for M = Ca, Sr, Ba, which suggests that the crystal field splitting and the center of gravity of Eu^{2+} are not very much influenced by the different crystal structures, but seems to be fixed by the $Si_2O_2N_2$ network.

The emission spectra of Eu^{2+}-doped $MSi_2O_{2-\delta}N_{2+2/3\delta}$ (M = Ca, Sr, Ba) show a typical broadband emission resulting from the 5d → 4f transition of Eu^{2+}, as shown in Figure 3. The position of the emission band differs with the type of M ions as generally found in Eu-doped alkaline-earth silicates and aluminates.[35−37] Excitation into the UV-blue range (370−450 nm), $M_{0.9}Eu_{0.1}Si_2O_{2-\delta}N_{2+2/3\delta}$ (M = Ca, Sr, Ba) yields efficient emission in the blue-green to yellow spectrum region. $BaSi_2O_2N_2$:Eu^{2+} shows a blue-green emission with a very narrow emission band at about 499 nm (FWHM ∼ 35 nm). $CaSi_2O_{2-\delta}N_{2+2/3\delta}$ Eu^{2+} shows a yellowish emission with a maximum at 560 nm. Similarly, the emission spectrum of $SrSi_2O_{2-\delta}N_{2+2/3\delta}$:$Eu^{2+}$ is composed of a broad emission band ranging from 530 to 570 nm depending on the Eu concentration and the O/N ratio (the

(34) Li, Y. Q.; De With, G.; Hintzen, H. T., to be published.

(35) Blasse, G.; Grabmaier, B. C. *Luminescent Materials*; Springer-Verlag: Berlin, 1994.
(36) Blasse, G.; Wanmaker, W. L.; Ter Vrugt, J. W.; Bril, A. *Philips Res. Rep.* **1967**, *23*, 189.
(37) Blasse, G.; Bril, A. *Philips Res. Rep.* **1968**, *23*, 201.

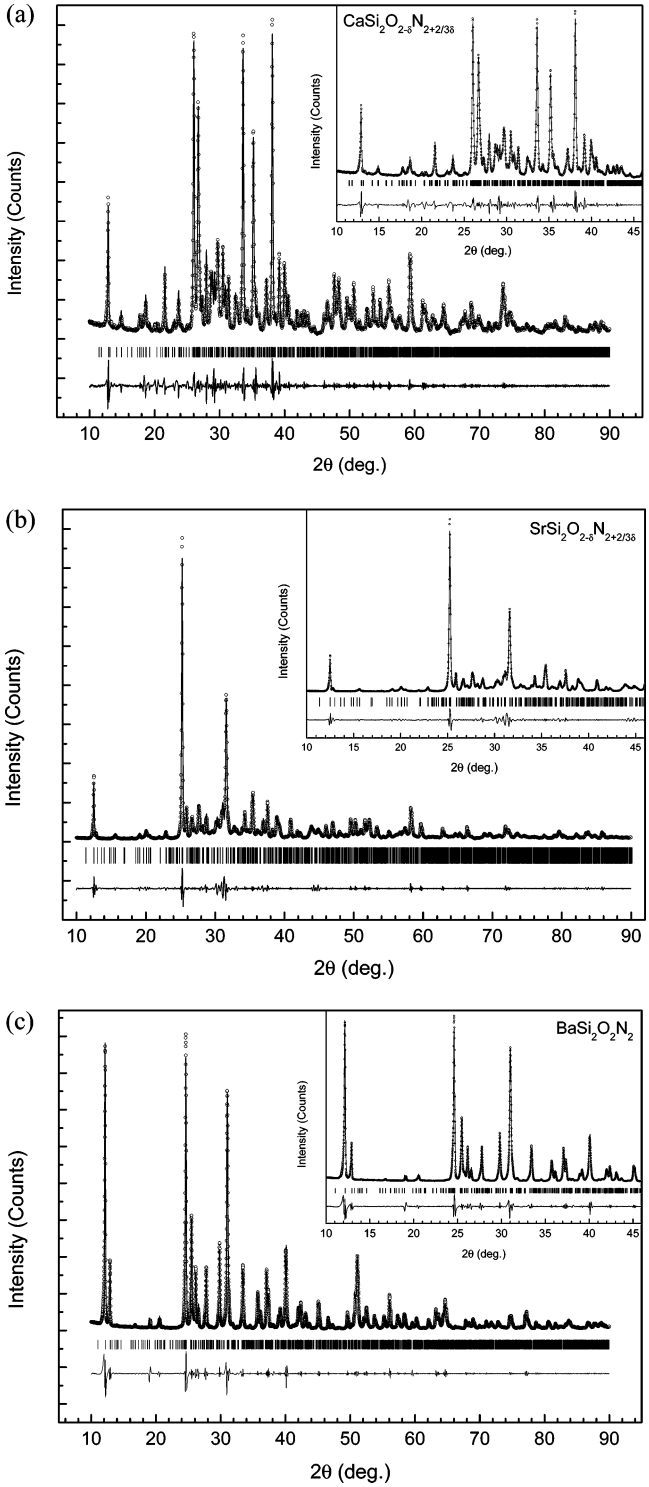

Figure 1. The observed (○) and simulated (solid line) X-ray powder diffraction pattern of $MSi_2O_{2-\delta}N_{2+2/3\delta}$: (a) M = Ca, (b) M = Sr, (c) M = Ba. The difference profile (observed − calculated) is shown at the bottom. The bars below the profile indicate the positions of all of the reflections allowed for $MSi_2O_{2-\delta}N_{2+2/3\delta}$.

emission band shows a red-shift with decreasing O/N ratio). As compared to the pure nitride compounds $M_2Si_5N_8$:Eu (M = Ca, Sr, Ba; $\lambda_{em} > 600$ nm),[10] the Eu^{2+} emission in $MSi_2O_{2-\delta}N_{2+2/3\delta}$ (M = Ca, Sr, Ba; $\lambda_{em} < 570$ nm) is at significantly lower wavelengths, suggesting that Eu is mainly coordinated to oxygen ions in $MSi_2O_{2-\delta}N_{2+2/3\delta}$. In accordance with this, the crystal structure determination of

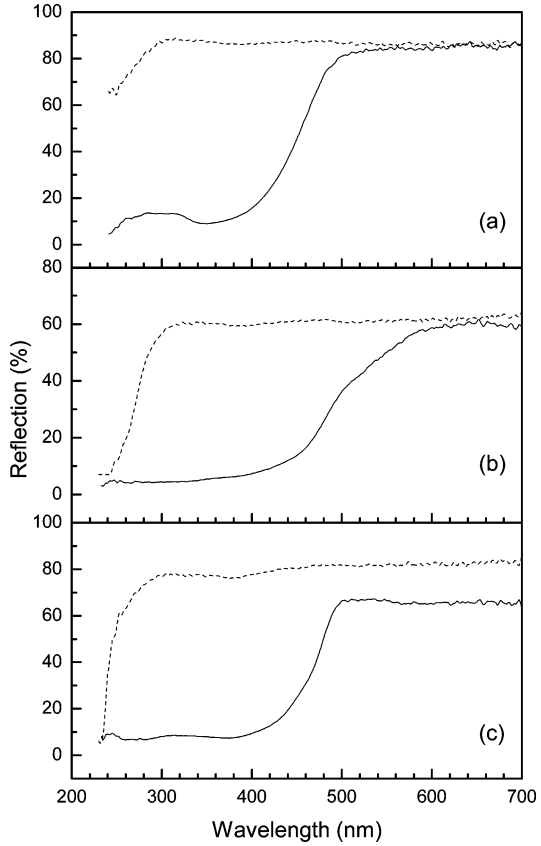

Figure 2. Diffuse reflection spectra of undoped (dashed line) and 10% Eu-doped (solid line) $MSi_2O_{2-\delta}N_{2+2/3\delta}$, (a) M = Ca, (b) M = Sr, (c) M = Ba.

$CaSi_2O_2N_2$ points to O atoms singly bonded to Si atoms, whereas the N atoms are triply bonded.[22]

The variation in position of the emission bands, while the excitation bands are at nearly the same energies, points to strongly different Stokes shifts depending on the type of M ion. Both $CaSi_2O_{2-\delta}N_{2+2/3\delta}$:$Eu^{2+}$ and $SrSi_2O_{2-\delta}N_{2+2/3\delta}$:$Eu^{2+}$ have a significantly larger Stokes shift than $BaSi_2O_2N_2$:Eu^{2+} (Table 3). The observation of the smallest Stokes shift for $MSi_2O_{2-\delta}N_{2+2/3\delta}$:$Eu^{2+}$ with the largest M ion (i.e., Ba) is consistent with our previous findings for Eu^{2+}- and Ce^{3+}-doped $MYSi_4N_7$ (M = Sr, Ba).[13,14] In addition to long-wavelength emission, this also results in lower quantum efficiency for Eu^{2+}-doped $MSi_2O_{2-\delta}N_{2+2/3\delta}$ (M = Ca, Sr) as compared to $BaSi_2O_2N_2$:Eu^{2+}. Besides a high quantum efficiency for UV-blue excitation (>60%), the smaller Stokes shift of $BaSi_2O_2N_2$:Eu^{2+} is responsible for the narrow emission band and results in improved thermal quenching behavior. Furthermore, having a somewhat larger crystal field splitting, the lowest energy excitation band of $BaSi_2O_2N_2$:Eu^{2+} at unusual long-wavelength (400−450 nm) is expected.

With an excitation maximum in the range of 430−460 nm, $MSi_2O_{2-\delta}N_{2+2/3\delta}$:$Eu^{2+}$ (M = Ca, Sr, Ba) can be efficiently excited in the blue region of the spectrum, which is very attractive for application in white-light LEDs. The chromaticity points of $M_{0.9}Eu_{0.1}Si_2O_{2-\delta}N_{2+2/3\delta}$ with different cation M (Ca, Sr, Ba) are shown in the CIE (1931) chromaticity diagram (Figure 4). For comparison, YAG:Ce^{3+} and $Sr_2Si_5N_8$:Eu^{2+} (excitation at 460 nm) are also plotted in Figure 4. Similar to YAG:Ce^{3+}, $MSi_2O_{2-\delta}N_{2+2/3\delta}$:$Eu^{2+}$ (M = Ca or Sr) in combination with a blue light source (InGaN

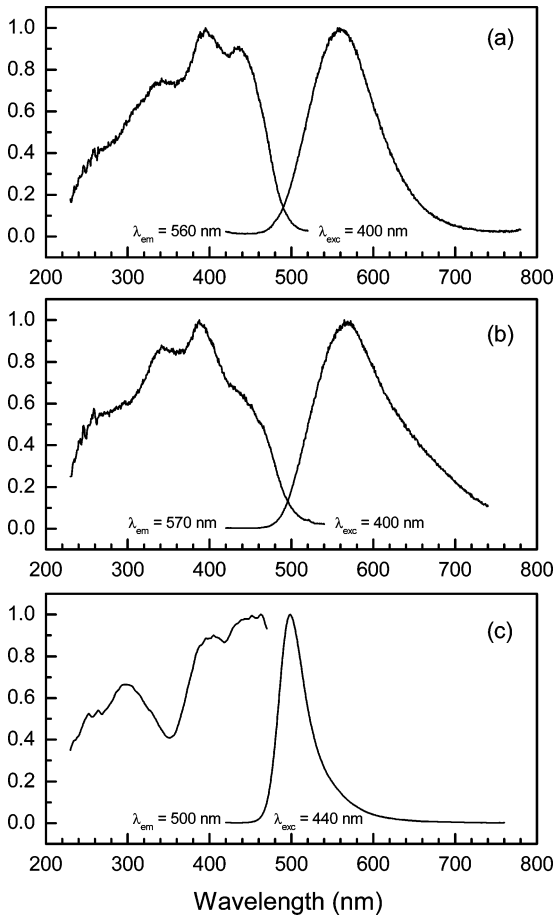

Figure 3. Excitation and emission spectra of $M_{0.9}Eu_{0.1}Si_2O_{2-\delta}N_{2+2/3\delta}$: (a) M = Ca, (b) M = Sr, (c) M = Ba.

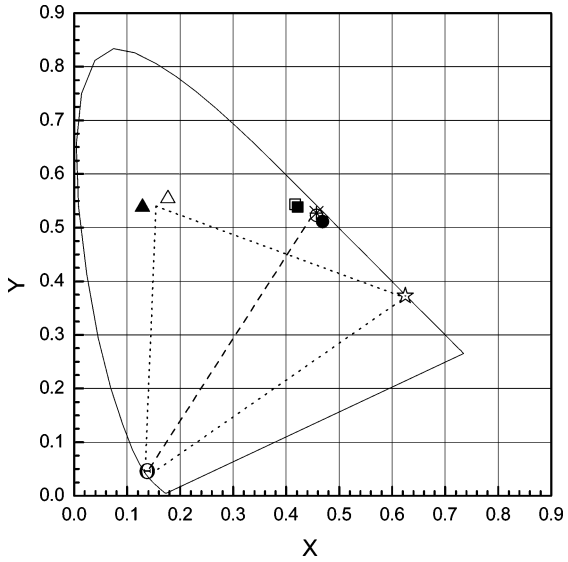

Figure 4. CIE chromaticity coordinates of $M_{0.9}Eu_{0.1}Si_2O_{2-\delta}N_{2+2/3\delta}$: (○, ●) $Ca_{0.9}Eu_{0.1}Si_2O_{2-\delta}N_{2+2/3\delta}$; (□, ■) $Sr_{0.9}Eu_{0.1}Si_2O_{2-\delta}N_{2+2/3\delta}$; (△, ▲) $Ba_{0.9}Eu_{0.1}Si_2O_2N_2$. Open symbols: λ_{exc} = 400 nm. Filled symbols: λ_{exc} = 460 nm. (∗) YAG:Ce^{3+} (λ_{exc} = 460 nm); (☆) $Sr_2Si_5N_8$:Eu^{2+} (λ_{exc} = 460 nm); (Θ) Blue InGaN chip.

chip) can generate white-light, while $BaSi_2O_2N_2$:Eu^{2+} (blue-green) together with $Sr_2Si_5N_8$:Eu^{2+} (orange-red) in combination with a blue light source also can give white-light in the RGB (red-green-blue) model which moreover has a high color rendering index (CRI), an extensive color range, and color stability as compared to the former case.[38]

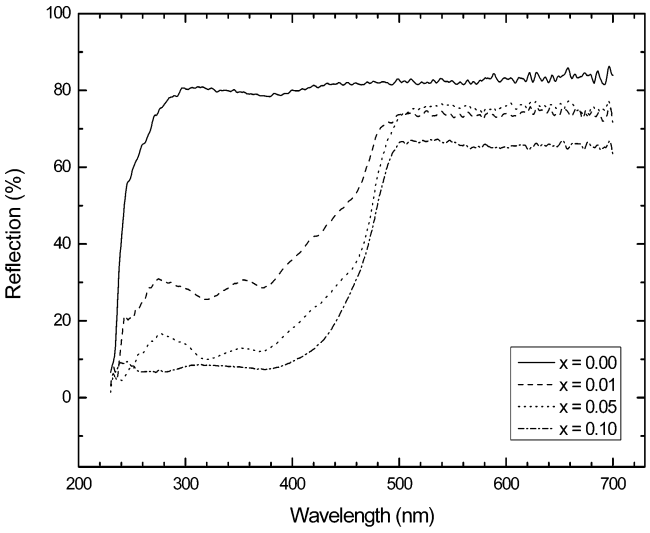

Figure 5. Diffuse reflection spectra of $Ba_{1-x}Eu_xSi_2O_2N_2$ (x = 0, 0.01, 0.05, 0.1).

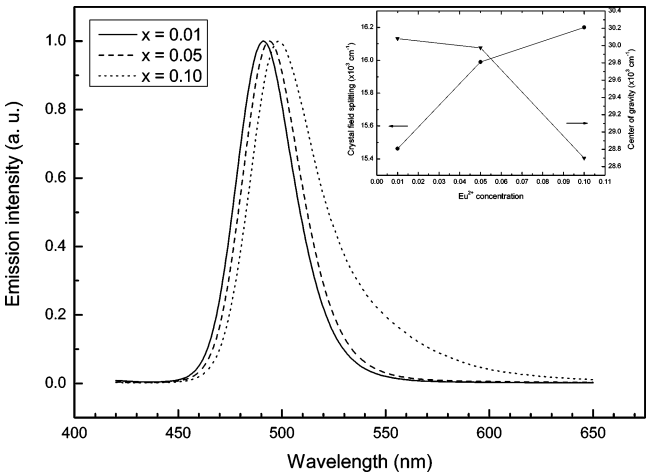

Figure 6. Emission spectra of $Ba_{1-x}Eu_xSi_2O_2N_2$ with varying Eu^{2+} concentration (λ_{exc} = 440 nm). Inset shows the dependence of the crystal field splitting and center of gravity of the 5d level on the Eu^{2+} concentration.

3.3. Effect of the Eu^{2+} Concentration on the Luminescence of $BaSi_2O_2N_2$:Eu^{2+}. As usual, with varying amounts of Eu^{2+} incorporated in the host lattice, the local surroundings around a substituted site will significantly change (i.e., bond length and angle as well as point symmetry), which eventually makes it possible to tune the luminescence properties. Similarly, it also can be realized by replacement of Ba by Ca and/or Sr. As a typical example, Figure 5 shows the relationship between the diffuse reflection spectra and the Eu^{2+} concentration of $BaSi_2O_2N_2$:Eu^{2+}. Obviously, with the Eu^{2+} concentration increasing from 1 to 10 mol %, as expected the onset of the Eu^{2+} absorption band extends at the long-wavelength side from 480 to 500 nm; meanwhile, the absorption intensity is enhanced in the visible range of 400−460 nm, which perfectly matches with the emission of the blue-InGaN based LEDs. Correspondingly, the excitation band also shifts to longer wavelength due to the increased crystal field splitting and covalency, as shown in an inset in Figure 6 (both crystal field splitting and center of gravity were derived from the excitation spectra), which results in a

(38) Hintzen, H. T.; Li, Y. Q.; Desling, A. C. A. PCT WO 2004/029177 A1.

red-shift of the emission band of Eu^{2+} from 490 to 500 nm (Figure 6). Because the estimated Stokes shift of $Ba_{1-x}Eu_xSi_2O_2N_2$ has not significantly increased from $x = 0.01$ to 0.1, this effect can be well explained by the replacement of the large Ba^{2+} ion by the smaller Eu^{2+} ion,[39] which results in the shrinkage of the Ba_{Eu}−O/N bond as we observed in other Eu^{2+}-doped systems.[13,14] In addition, the emission red-shift can also be augmented by self-absorption at higher Eu^{2+} concentration.

4. Conclusions

Eu^{2+}-activated $MSi_2O_{2-\delta}N_{2+2/3\delta}$ (M = Ca, Sr, Ba) has been synthesized and characterized using X-ray powder diffraction as well as reflectance, excitation, and emission spectroscopy. A new oxynitride compound $BaSi_2O_2N_2$ was obtained in the $BaO-SiO_2-Si_3N_4$ system. $BaSi_2O_2N_2$ crystallizes in a monoclinic unit cell with the lattice parameters $a = 14.070(4)$ Å, $b = 7.276(2)$ Å, $c = 13.181(3)$ Å, $\beta = 107.74(6)°$. For excitation with radiation in the UV-blue range, $MSi_2O_{2-\delta}N_{2+2/3\delta}:Eu^{2+}$ exhibits efficient blue-green emission at 490−500 nm for M = Ba, whereas yellow and green-yellowish emission at 560 and 530−570 nm were found for M = Ca and M = Sr, respectively. With an intense absorption and excitation band in the UV-blue spectral region (370−460 nm), combined with a high quantum efficiency, these materials can be used as novel conversion phosphors for white-light LEDs.

CM050175D

(39) Shannon, R. D. *Acta Crystallogr.* **1976**, *A32*, 751.